MECHANICAL PERFORMANCE OF DISSIMILAR STRUCTURAL STEEL LAP JOINTS: EXPERIMENTAL TEST SUPPORTED WITH NUMERICAL SIMULATIONS

MARTIN DOSTAL[1], HANA SEBESTOVA[2], JINDRICH VILIS[3], MAREK SLOVACEK[1], PETR SVOBODA[1], MARTIN KLIMES[3]

[1]Brno University of Technology, Faculty of Mechanical Engineering, Institute of Manufacturing Technology, Brno, Czech Republic

[2]Institute of Scientific Instruments of the Czech Academy of Sciences, Brno, Czech Republic

[3]Faculty of Military Technology, University of Defence, Brno, Czech Republic

DOI: 10.17973/MMSJ.2026_11_2026093

e-mail: 217110@vutbr.cz

This study presents a comprehensive analysis of dissimilar lap joints made of S235JR (4 mm) and S355MC (3 mm) structural steels using G3Si1 (1 mm) filler wire. Welding was performed using the MAG (Metal Active Gas) process in CMT (Cold Metal Transfer) mode. Four specimens were welded with different heat inputs (Q) from 0.4 to 0.6 kJ/mm. The welding parameters had a significant effect on the weld geometry, particularly on the weld height, which increased with higher Q, and on undercuts, which decreased with higher Q. Specimens with lower Q contained undercuts that served as crack initiation sites during tensile tests. The specimen with the highest Q had minimal undercuts, and the fracture occurred within the base material (BM). The fatigue behaviour of these joints was evaluated using FAT curve analysis, achieving values in the category 614 (FAT36 to FAT60). An analysis of the welding process was also performed using the finite element method (FEM), which generally confirmed the experimental results. The results demonstrated good correlation between the experimental results and the numerical simulations.

KEYWORDS

Structural steels, dissimilar lap joints, CMT welding, Numerical simulations, Fatigue

1 INTRODUCTION

Lap joints in structural steels represent a common joint configuration in industrial practice, particularly in cases where simple joint geometry, low production costs, and high assembly speed are required. However, for structural steels S235, S355, and especially fine-grained variants such as S355MC, it is necessary to consider not only achieving the required strength but also the size of the heat-affected zone, weld pool stability, deformation, and the resulting fatigue resistance of the component. These aspects are particularly important in MAG (Metal Active Gas) welding because, although the process is technologically robust and widely used, it is sensitive to the choice of metal transfer mode, welding speed, and heat input. [Oliveira 2024, Stanciu 2017, Schmidt 2025]

S235 steel generally offers good weldability and relatively low susceptibility to the formation of hard structures in the heat-affected zone. However, in lap joints, the disadvantages associated with higher heat input may still arise, particularly greater distortion and a local decrease in joint quality at the transition from the weld to the base material. The situation is more complex with S355 steel, as the higher strength level is associated with a more sensitive response to the welding cycle and a greater need to control residual stresses and microstructural changes. S355MC, a thermomechanically rolled fine-grained steel, deserves special attention, as even relatively mild heat input can lead to significant changes in local mechanical properties in the HAZ. [Schmidt 2025, Kubicek 2016] G3Si1 filler material is commonly used for these materials. It is intended for unalloyed and low-alloy structural steels.

The technical literature repeatedly documents that the quality of a MAG weld depends on proper parameter settings, arc stability, and heat input control. However, for thinner sheets and components sensitive to deformation, the conventional MAG process may be limited by the risk of overheating or unsatisfactory bead geometry. In the case of lap joints, weld quality is also significantly influenced by the process's ability to ensure uniform fusion of both sheets without a wide HAZ. [Stanciu 2017, Muncut 2015, Nagasai 2024]

Scientific studies show that, compared to conventional synergistic pulsed MAG welding, CMT can achieve a smaller bead width and a smaller heat-affected zone, particularly when welding thin steel sheets. This property is significant for lap joints because it reduces the likelihood of distortion, burn-through, and excessive HAZ development, which is particularly critical for thinner sheets or where high dimensional stability is required. [Stanciu 2017, Oliveira 2024, Nagasai 2024]

In the case of S235 and S355MC, control of heat input is particularly crucial, as local changes in microstructure can affect not only the static strength but also the fatigue properties of the joint. The literature on residual stresses in S235 and S355 joints shows that MAG welding without sufficient clamping leads to significant stress states, which can have a direct impact on the service life of the structural component. In this context, CMT is attractive due to its lower heat input and potentially lower development of residual stresses. [Mueller 2022]

In terms of mechanical properties, not only static strength but also resistance to cyclic loading is critical for lap joints. Fatigue failure in welded lap joints is most often initiated in the weld toe or at the weld root, with local stress concentration, the dimensional geometry of the joint, surface quality, and residual stresses after welding playing a decisive role. In combined or heterogeneous joints, the fatigue life also varies depending on the difference in thicknesses and the degree of loading eccentricity, as the joint operates under combined tension and bending [Hobbacher 2025, Macdonald 2011, Lang 2025].

For structural steels S235 and S355, both experimental and numerical studies show that residual stresses after welding can reach values close to the yield point and significantly reduce the fatigue life of the component [Mueller 2022, Lang 2025]. This effect is particularly pronounced in lap joints, as the joint is geometrically sensitive to changes in the weld root and to local discontinuities at the transition between the plates and the fillet [Hobbacher 2025, Macdonald 2011]. Therefore, for the evaluation of these joints, it is appropriate to combine classical mechanical tests with an assessment of macrogeometry, hardness profile, microstructure, and fatigue behaviour.

[Stanisz 2022, Lang 2025] Furthermore, regarding dissimilar lap joints, it is important to note that differences in sheet thickness or the strength of the base materials alter the distribution of forces in the joint area. Higher strength in one of the sheets does not automatically imply higher fatigue resistance of the assembly, as the decisive factor is often the local stress in the vicinity of the weld, not merely the nominal strength of the base material. For similar joints, it has been repeatedly demonstrated that fatigue cracks initiate predominantly in the weld toe region, or at the weld root, and that their propagation is strongly influenced by the direction of loading, surface quality, and the extent of geometric discontinuities present. [Hobbacher 2025, Macdonald 2011]

Numerical analyses in progressive design have become an indispensable tool in modern structural design. However, the accuracy of numerical analyses results depends largely on the quantity but also the quality of the available input data. Standard numerical simulations for welding procedures are unable to predict the occurrence of defects such as cracks or undercuts, etc. On the other hand, these modern tools enable the prediction of the size of the heat-affected zone, hardness profiles, stress distributions (residual stresses, etc.), material deformation, structural changes, or, for example, local values of mechanical properties. The Goldak model, an analytical heat source in the SYSWELD simulation software suite for MAG (Metal Active Gas) welding, was used, this model mathematically approximates the arc energy input using a double ellipsoidal heat source, which is the most widely adopted model. It considers the asymmetrical temperature distribution in the molten pool—the front part of the weld is shorter and steeper, while the rear part is longer and cools gradually, as is the case with MAG welding. [Kik 2024, Peric 2021, Mroz 2023]

Despite the widespread application of CMT welding in structural steel fabrication, limited information is available on the fatigue behaviour of dissimilar lap joints combining conventional S235JR steel and thermomechanically rolled S355MC steel. While previous studies have mainly focused on weld formation, heat input optimisation and static mechanical properties, considerably less attention has been paid to the relationship between weld geometry, undercut formation and fatigue performance. Furthermore, only a limited number of studies combine experimental evaluation with numerical prediction of thermal cycles, hardness evolution and residual stress development.

The objective of this work was therefore to evaluate the influence of heat input on weld geometry, hardness distribution, tensile behaviour and fatigue performance of dissimilar S235JR/S355MC lap joints produced by CMT welding. Experimental observations were subsequently compared with numerical simulations performed using SYSWELD software.

2 MATERIALS AND METHODS

2.1 Materials

The experimental welding research described in this paper was conducted at a welding laboratory at the Institute of Manufacturing Technology, FME, BUT. Two different base materials were used in this study. The first was standard S235JR steel (material no. 1.0038) with a thickness of 4 mm. The second type of material was 3 mm thickness steel S355MC (material number 1.0976). Material properties for both used steels are shown in Table 1 and Table 2. G3Si1 filler metal (equivalent G 42 4 C1/M21 3Si1) with a wire diameter of 1 mm was used for welding. Its mechanical properties and chemical composition are taken from the material certificate, see Tab. 1.

	Re [MPa]	Rm [MPa]	A [%]	HBW
S235JR	297	400	33	120
S355MC	390	490	27	155
G3Si1	440	540	26	-

Table 1. Mechanical properties

	C [%]	Si [%]	Mn [%]	S and P [%]	Fe [%]
S235JR	0.19	-	1.3	max. 0.012	rest
S355MC	0.09	0.25	1.4	max. 0.009	rest
G3Si1	0.1	0.8	1.5	max. 0.010	rest

Table 2. Chemical composition

The design of the welded joint is shown in Figure 1. The joint was designed with a 20 mm overlap. The total width of the joined materials after welding is 250 mm. The sheet metal blanks were cut.

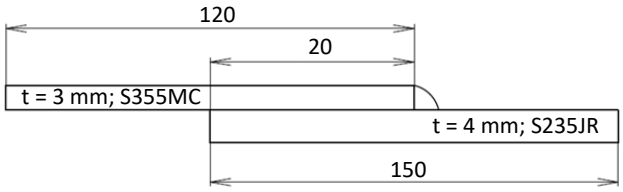


Figure 1. Dissimilar lap joint – S355MC and S235

2.2 Welding conditions

The lap joints were welded using the MAG (Metal Active Gas) method with CMT mode (Cold Metal Transfer) with Fronius TransPuls Synergic 3200 CMT welding power source. A KUKA KR 5 arc industrial robot was used for the experiment, along with an experimental welding fixture designed to fully clamp the workpieces (Figure 2). This figure also illustrates the welding torch position settings for the welding procedure. The torch position during welding was adjusted to reduce the occurrence of undercuts. An Ar+CO_2 shielding gas mixture in an 82/18 ratio was used for welding, with a gas flow rate of 19–21 l/min. This shielding gas mixture is standard for welding these steels.

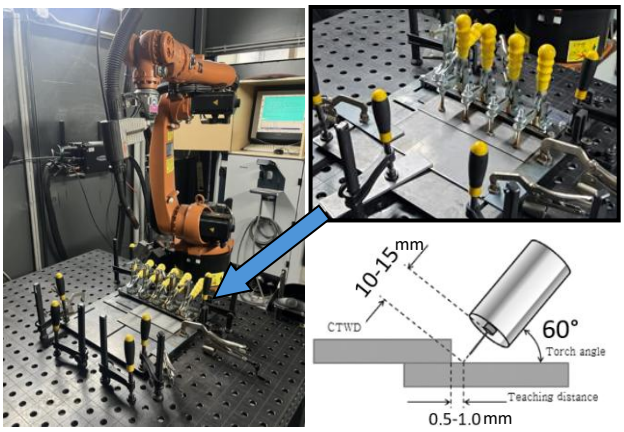


Figure 2. Dissimilar lap joint

Table 3 presents the welding parameters (for each sample) which were used in the experiment. The heat input (Q) was calculated using the typical absorption efficiency for the MAG method, which is 0.8 (80 %) The calculated carbon equivalent (CEV) was approximately 0.40 for S235JR steel and 0.32 for

S355MC steel according to the IIW formula. Both values indicate good weldability and confirm that no preheating was required under the selected welding conditions.

No.	I [A]	U [V]	v [m/min]	W [m/min]	Q [kJ/mm]
S1	225	25.7	10.0	8.0	0.46
S2	250	26.8	10.0	9.1	0.54
S3	275	27.2	10.0	9.9	0.60
S4	200	24.7	10.0	7.7	0.40

I – Current; U – Voltage; v – velocity; W – Filler wire feed rate

Table 3. Welding parameters

The selected welding parameters correspond to a heat input range between 0.40 and 0.60 kJ/mm. This interval was chosen to investigate the effect of heat input on weld geometry, undercut formation and resulting mechanical properties while maintaining stable CMT transfer conditions.

2.3 Methods of process and inspection

The welded specimens and base metal blanks were cut on a saw cooled by a water-emulsion coolant and then ground and polished. Polished bead cross-sections and base material also were etched with 2% Nital reagent for 10 s to reveal the macro and microstructure of the substrate. The samples were examined using a Keyence VK-X1000 laser scanning confocal microscope.

The Vickers hardness tests were performed under a load of 1 kgf (HV1). The measurements were taken on polished samples. It was measured using a hardness tester QATM Qness 60A+ EVO. The measurements were taken at a depth of 1 mm below the surface. The measurement was taken in a single line across the entire weld joint (Fig. 3) and both base materials. Spacing between linear measurements (indents) was 0.5 mm for WM and HAZ and 1 mm for BM. The hardness maps were generated with a grid spacing of 0.5 mm × 0.5 mm. Hardness measurements met the requirements of EN ISO 9015-1.

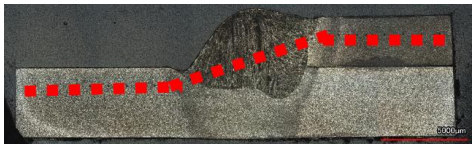


Figure 3. Hardness profile line

Tensile tests were conducted on the welded lap joints and also for both base materials. Tensile testing was conducted using a Zwick/Roell Z100 machine equipped with a load cell for up to 100 kN capacity. The machine was also equipped with a high precision extensometer for contactless displacement measurements. The specimens for the tensile tests were cut to size and then milled. The dimensions of the test specimens are shown in Figure 4. It was similar for welds and basic material. The specific dimensions of the specimens were measured with a caliper immediately before the test. Since the dissimilar lap weld was an unsymmetrical joint, the bending loads were minimized by using pads during testing. The test conditions were chosen in accordance with the EN ISO 6892-1 standard.

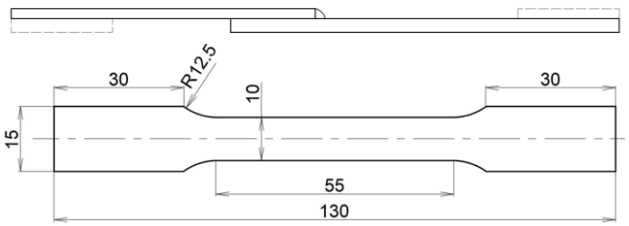


Figure 4. Specimen for tensile test

The fatigue testing was carried out on a Zwick/Roell Vibrophore 250 HFP 5100 (Fig. 5) with the maximum load capacity 250 kN. The specimens for the fatigue tests were cut to size and then milled. The dimensions of the specimen are shown in Figure 6. Based on the initial conditions (tested materials, type of weld joint etc.) and available data (tensile testing etc.), the strain amplitudes of the fatigue loading were determined to 25, 30, 60, 75 and 85 MPa with stress oscillation R = 0.1 (amplitude; asymmetry of the cycle). The strain values were evaluated in relation to the cross-sectional area of the S355MC material. The specimens exhibited slight post-weld distortion, despite full clamping. Therefore, during testing, bending moments (forces) also act on the specimen.

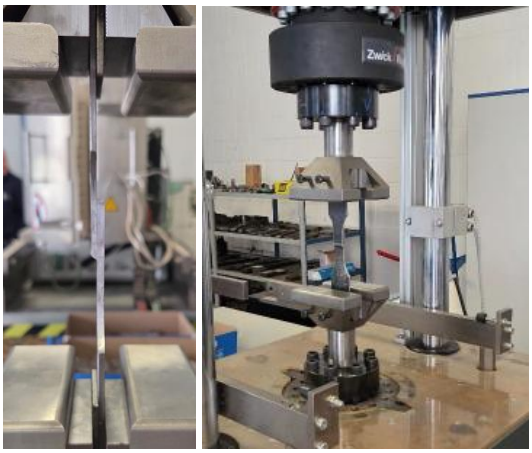


Figure 5. Fatigue testing

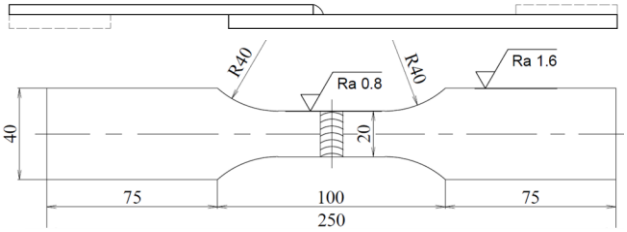


Figure 6. Specimen for fatigue test

The chemical composition of the base materials was taken from the inspection certificates and then verified by spectrochemical analysis. The analysis was performed using the Q4 TASMAN Spectrometer.

3 EXPERIMENTAL RESULTS

3.1 Microstructural and macrostructural analyses

Both base materials are conventional structural steels with a ferritic-pearlitic microstructure. The S355MC material is thermomechanically processed, and its grain structure is significantly finer than the grain structure of the S235 material, see Fig. 7. A banded microstructure resulting from the rolling process was observed in both materials.

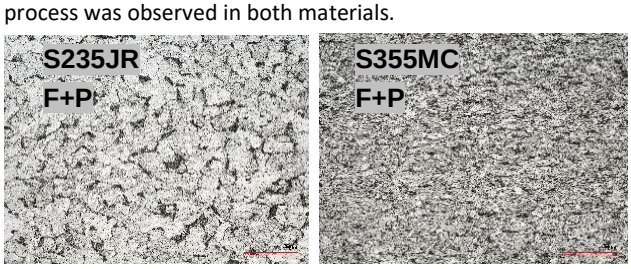


Figure 7. Materials S235JR (left) and with finer grains S355MC (right)

The macrostructural features of the weld beads obtained under different heat inputs are presented in Figure 8. The welds were evaluated in accordance with ISO 5817, quality level C. Although all welds satisfied the requirements regarding weld reinforcement, none of the specimens fulfilled the acceptance criteria for undercuts. The measured weld reinforcement increased with increasing heat input, whereas the severity of undercuts decreased. Since undercuts represent geometric discontinuities acting as local stress concentrators, their reduction is favourable from the perspective of fatigue performance. All welds exhibited a certain degree of geometric asymmetry, which resulted from the torch inclination adopted to minimise undercut formation. Furthermore, increasing heat input promoted deeper penetration and improved fusion between the weld metal and the base materials. The relationship between heat input and the resulting weld geometry is illustrated in Figure 8.

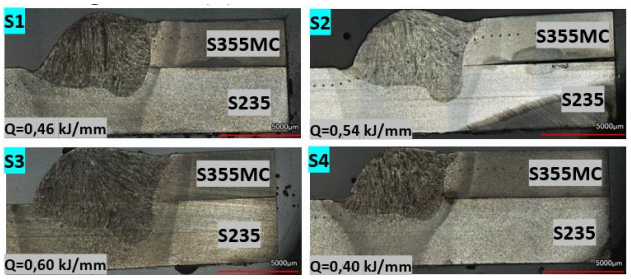


Figure 8. Macrostructure of welded joints

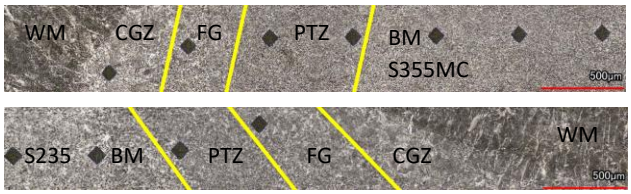
A quantitative evaluation of the weld geometry is summarised in Table 4. Increasing heat input resulted in greater weld reinforcement and penetration depth, whereas the severity of undercuts decreased. The lowest undercut depth was observed for sample S3 (Q = 0.60 kJ/mm), while the most pronounced undercuts were found in the specimens produced with lower heat inputs. These geometric differences subsequently influenced the crack initiation behaviour observed during tensile and fatigue testing.

No.	Q [kj/mm]	Weld reinforcement [mm]	Penetration depth p [mm]	Undercut depth u [mm]
S1	0.46	Medium	Medium	High
S2	0.54	Medium	Medium	Medium
S3	0.60	High	High	Low
S4	0.40	Low	Low	High

Table 4. Geometrical parameters of the welded joints obtained at different heat inputs

The values listed in Table 4 are consistent with the macrostructural observations shown in Figure 8. Higher heat input promoted deeper penetration and increased weld reinforcement, while simultaneously reducing undercut severity. From the perspective of fatigue performance, the reduction of undercuts is particularly important, as these features act as local stress concentrators and preferential crack initiation sites.

The transition between the different regions of the weld joint, from the base material to the weld metal, is shown in Figure 9. Due to the utilization of the CMT mode, a narrow HAZ was achieved. This is because CMT mode applies less heat to the weld than standard modes. A tighter HAZ has a positive effect on the welded joint of structural steels (less deformation and grain coarsening, less stress, etc.). The process achieved the expected results in terms of the welded materials and the technology used.



Legend: CGZ – Coarse grain zone, FG – fine-grained zone, PTZ – partially tempered zone, WM – Weld metal, BM – base material

Figure 9. Macrostructure detail of weld joint (sample 1) with the results of the numerical simulation

The weld metal exhibits an as-cast microstructure (Fig. 10) with a microstructure mainly composed of bainite and acicular ferrite. Weld S1 was evaluated. For the other samples, given that they consist of the same materials, similar microstructural features are anticipated (bainite + acicular ferrite), although there may be minor differences in the relative proportions of the phases or in grain size.

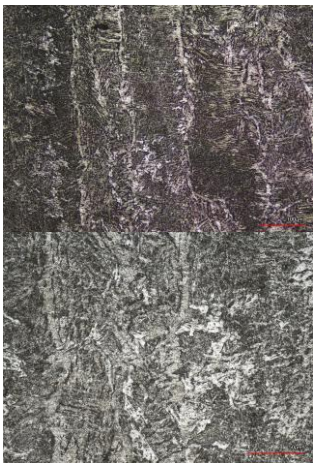


Figure 10. Weld metal (left side mg. 20x and right side 50x)

3.2 *Hardness and tensile testing results*

The hardness profile is shown in Figure 11. As shown, the different heat inputs did not significantly affect the hardness values (HV). The differences in the average hardness values of the weld metal were within the experimental scatter of the measurements. The results show that there is no degradation of the HAZ. Therefore, there is no decrease in HV compared to the BM. Due to the high cooling rate, the HV values in the HAZ are higher than those in the BM. As expected, base materials S355MC exhibits higher HV1 values than S235JR.

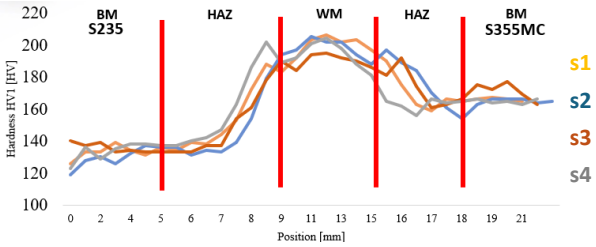


Figure 11. Hardness profile – experimental measurements

Regardless of the applied heat input, all hardness profiles exhibited a comparable character. The highest hardness values were consistently measured within the weld metal, while the hardness gradually decreased towards both base materials. No measurable softening was observed in the heat-affected zone. This indicates that the selected welding conditions did not lead

to degradation of the thermomechanically processed S355MC microstructure.

The hardness map was also evaluated and is shown in Figure 12. The results are similar to the hardness measurements taken across the profile. The figure also includes a comparison of materials in terms of their mechanical properties, which in turn affects their hardness. Based on this, the results confirmed that the weld metal achieves the highest hardness values.

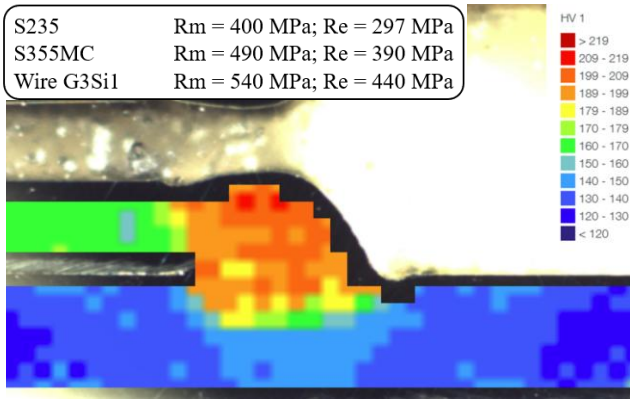


Figure 12. Hardness map

During the tensile tests the material failure occurred in the notch (undercuts area) of samples S1, S2, and S4 at the HAZ of the S355MC, see Fig. 13 and 14). In the area of undercuts there is also a fusion line area, where a significant local decrease in properties observed. At this area, there was also a local reduction in material thickness to 3 mm. In this configuration, this thinner material is more sensitive to notch effects than the 4 mm thick S235JR steel, which is why the crack originated primarily here.

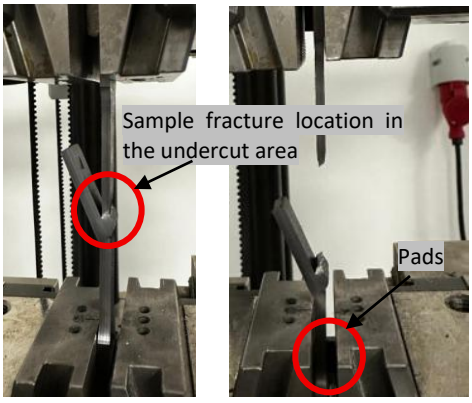


Figure 13. A demonstration of the tensile testing process

In contrast, in sample S3, the fracture occurred in the BM of the S355MC material, rather than in the undercut as in the other samples. This sample had the lowest undercut and its effect was therefore not observed as it was in samples S1, S2, and S4.

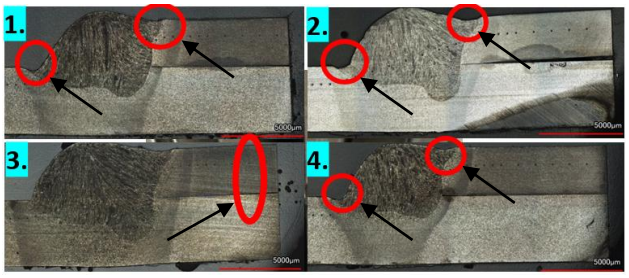


Figure 14. Locations of sample fractures during tensile tests

The forces (F_m) required to break the individual samples are listed in the Table 5. The differences between the results are negligible. For dissimilar lap joints, the breaking force is specified instead of the standard tensile strength (Rm) due to differences in cross-sectional area. The materials used have different thicknesses, including the weld, defining a single representative cross-sectional area remains ambiguous due to geometric variations.

No.	Q [kJ/mm]	F_m [kN]
S1	0.46	14.1
S2	0.54	14.2
S3	0.60	14.4
S4	0.40	14.1

Table 5. A comparison of the heat input with the force required to break the specimens

Although the fracture locations differed among the individual specimens, the maximum forces remained within a very narrow range. The difference between the highest and lowest recorded value did not exceed approximately 2 %. The results therefore suggest that the overall load-bearing capacity of the joint was only weakly affected by the observed geometric imperfections. Their influence became apparent primarily through the crack initiation location rather than through a reduction in the ultimate load.

3.3 Fatigue analysis

Specimen S3 was selected for fatigue testing due to its optimized weld geometry (fewest undercuts) and performed well in tensile tests. The welds were evaluated in accordance with ISO 5817, quality level C. The results are based on the S355MC material cross-section, see Table 6. The results were then also evaluated using the FAT curves (Fig. 16) specified in the IIW Fatigue Recommendations document, which is based on the ČSN EN 1993-1-9 standard [Hobbacher 2025]. In this standard, the vertical axis of the FAT curve graph shows the amplitude deviation (the total strain range), which is equal to twice the tested strain amplitude. The comparable lap joint specified in the standard is number 614. This number specifies a stress of 63 MPa (FAT 63) in the BM at the weld interface (crack at the weld toe) and a stress of 36 MPa (FAT 36) in the effective cross-section of the weld (crack at the weld root). Four of the tested specimens exhibited fatigue failure (or crack initiation) at the weld toe, one showed no visible damage, and one specimen exhibited damage at the weld root. The curve illustrating the fatigue behaviour of the tested specimen is shown in Figure 15.

σ_A [MPa]	Cycles N [-]	Min. N, FAT 36 [-]
25	1,165,830	746,496
30	943,598	432,000
60	106,572	54,000
75	37,592	27,648
85	11,876	18,993

Note: The testing was conducted with a cycle asymmetry of 0.1.

Table 6. Results - fatigue testing for sample S3

A markedly different behaviour was observed under cyclic loading. In contrast to the tensile tests, fatigue crack initiation was strongly associated with local geometric discontinuities at the weld toe. Most failures originated in regions affected by undercuts (significant notch effect), indicating that local stress

concentration effects governed fatigue life to a significantly greater extent than the nominal strength of the welded joint.

For the evaluation, it is essential that the specimens exceed the FAT 36 value. Most of the tested samples safely exceeded the number of cycles defined by the FAT 36 reference curve across the entire range of loading amplitudes. Only the sample tested at the highest amplitude failed (85 MPa). However, this amplitude was at the upper limit of the initial assumptions (based on tensile tests and material properties), so this result was expected.

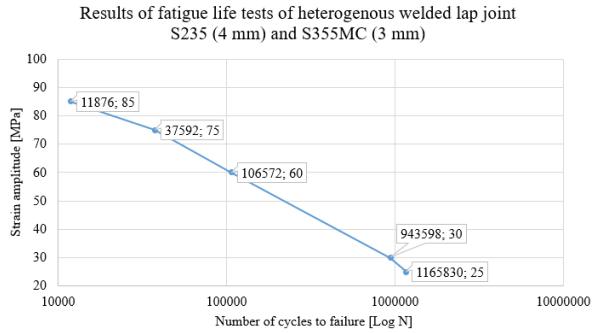


Figure 15. Fatigue life test curve

It follows that although the test specimens did not fail at the root, their actual endurance reliably exceeded the minimum required by the standard for a root crack. This means that, in terms of stress in the effective cross-section of the weld, the designed joint and the selected welding parameters are satisfactory.

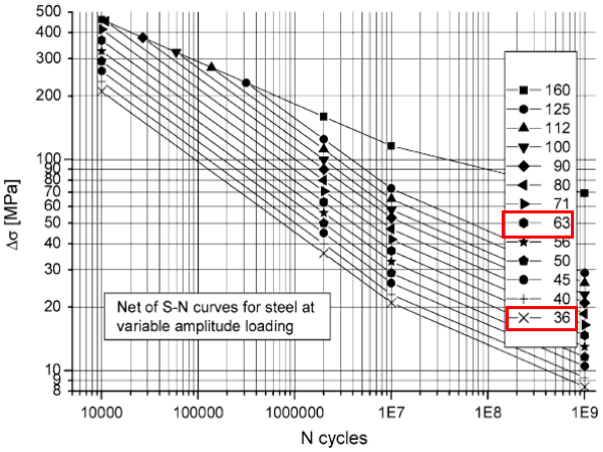


Figure 16. FAT curve acc. IIW recommendations [Hobbacher 2025]

The fatigue results presented in this work should be regarded as an initial assessment of the investigated joint configuration. A more detailed evaluation of crack initiation mechanisms, crack propagation behaviour and statistical fatigue life assessment would require a substantially larger testing programme and therefore remains a subject for future investigation.

4 NUMERICAL SIMULATIONS

4.1 FEM model

Numerical simulations were performed using Sysweld software. The FEM model (Finite element method) was used as the numerical model. The geometry for the analysis was identical to the dimensions of the blanks used in the experiment (Fig. 17). The Visual-mesh application (a tool for creating 2D and 3D meshes) was used for the modelling. The mesh density decreases in the direction away from the weld due to the computational complexity of the calculation itself and the decreasing temperature gradient.

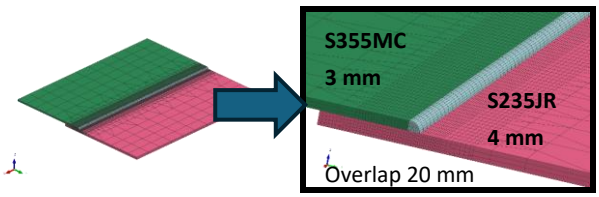


Figure 17. Design and mesh of a welded joint in the software Sysweld

The material models for both steels were selected from the software library, and their material properties were adjusted to correspond to their actual values (based on the analysis conducted). The numerical models also included the necessary boundary conditions (elements into which heat flows, and the inclusion of clamps). The clamping of the metal sheets corresponded to the actual conditions, and it was released after 1,000 seconds to unload the weldment and show the deformations. The welding was performed without preheating, and heat transfer was set to air. The Goldak double ellipsoidal heat source model was used. The heat input (Q) was calculated using the typical absorption efficiency 0.8.

The hardness results from the numerical simulations were measured in two methods (map and profile). The data are presented in the form of hardness values across the profile and a map. The joint cross-section was measured along four lines point by point (element by element) across the model's mesh. The hardness map is measured on all elements of the mesh.

4.2 Numerical simulations results

Numerical simulations were used for only one reference sample – sample S1, see Tab. 3; Q = 0.46 kJ). This specimen was considered representative of the investigated welds, as only minor differences were observed in hardness distribution and tensile behaviour among the individual samples, with all measured values remaining within the scatter expected for a single weld. Figure 18 shows the course of the welding simulation and the temperature field for the given settings, as well as an illustration of how the heat is conducted into both materials. Due to their similar chemical composition, heat conduction in both materials is very similar.

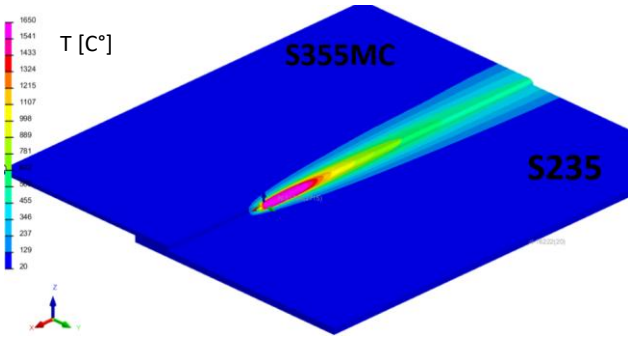


Figure 18. Design of a welded joint in the software Sysweld

Figure 19 shows a visualization of the HAZ region and its range. In areas where the maximum temperature did not reach 720 °C (Ac1), austenitization did not occur, and the original structure of the base material remained fully intact (purple colour) and thus visually defines the outer edge of the HAZ. In contrast, the elements representing areas where complete austenitization and a complete structural change occurred are shown in blue.

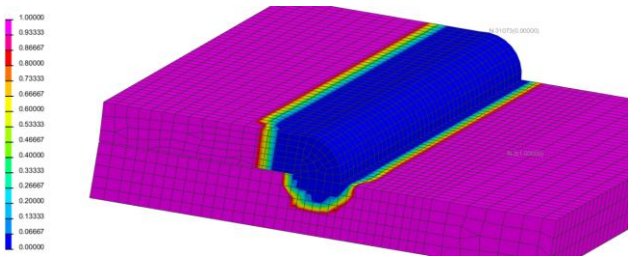


Figure 19. Visualization of HAZ and the original phases

Figures 20 and 21 show the proportions of the individual phases present in the material after welding. These figures represent the ratio of the phase under examination to the remaining structures. The results are plotted in a cross-section of the weldment. As can be seen, the highest proportion of ferrite is found in S355MC steel. In contrast, the highest proportion of bainite is found in S235 material.

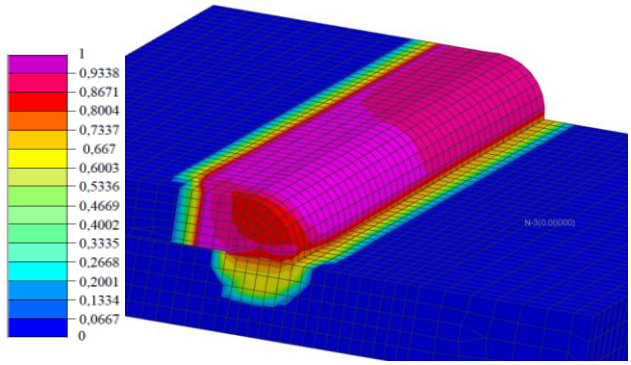


Figure 20. Ferrite fraction

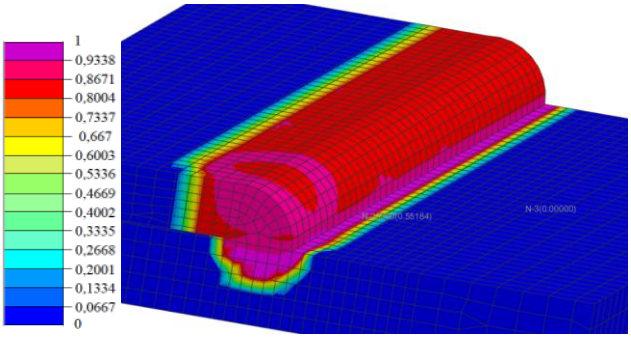


Figure 21. Bainite fraction

The resulting hardness values of the welded joint are shown in Figure 22. The maximum hardness (approximately 200 HV) is measured in the weld metal and gradually decreases toward the base metals until it reaches the hardness values of both base metals.

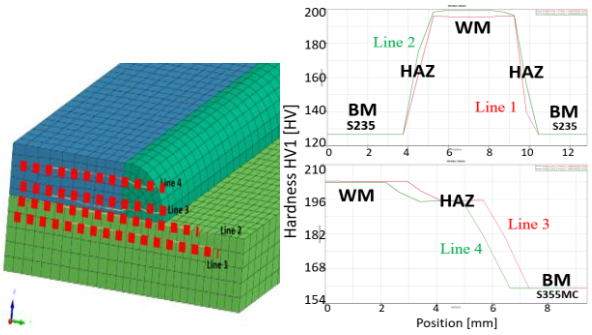


Figure 22. Hardness profile – numerical simulations

The results of the hardness map are visualized throughout the simulated model, and the hardness values correspond to the readings from hardness measurements taken along a cross-section of the profile. Since the hardness measurements across the weld joint profile were quite similar, only one reference sample (S1) was selected for the hardness map. Figure 23 also shows a comparison of hardness with the mechanical properties of the individual materials. The filler material used, G3Si1, has the highest strength properties, which corresponds with the location of the highest hardness in the weld metal.

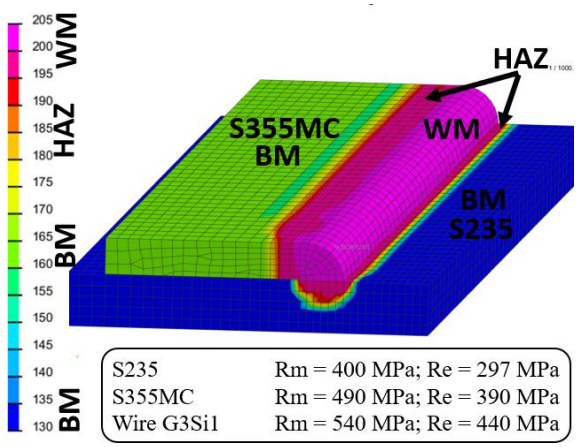


Figure 23. Hardness map

Deformations were then calculated throughout the entire volume of the weldment (Fig. 24). Due to the asymmetry of the lap joint and the temperature gradient, angular deformation occurs throughout the weldment, along with bending deformation along its sides. The greatest deformation is found on the left side.

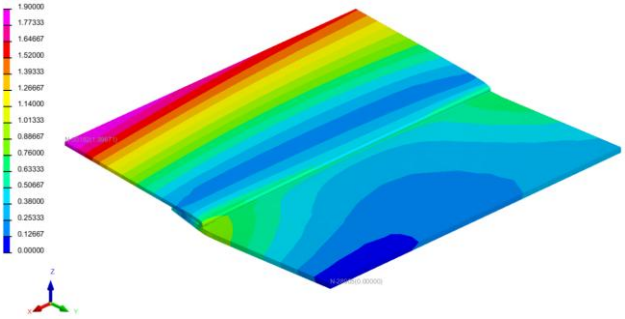


Figure 24. The results of normal deformations

Figure 25 provides an overall picture of the stress distribution. The highest values of equivalent stress (von Mises stress) are concentrated directly in the weld and in a narrow zone of the heat-affected zone (HAZ). Since the maximum stress of approximately 530 MPa reaches or exceeds the yield strength of the base materials used, this means that the material in this zone underwent plastic deformation during the thermal cycle, and residual stresses remained in it after cooling. In the more distant base material, the stress decreases because only elastic deformations occurred there. The nature of the residual stresses is shown in Figure 26. Positive values, i.e., tensile stresses, are found in the vicinity of the weld, whereas compressive (or negative) stresses are found at the edges of the weldment.

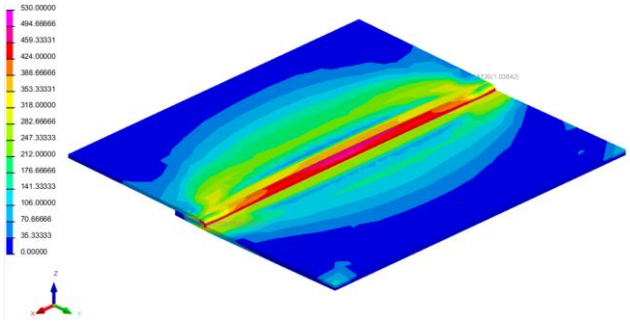


Figure 25. Equivalent stress (von Mises stress)

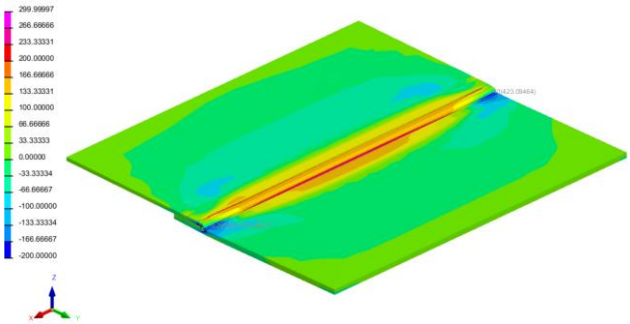


Figure 26. Residual stresses

5 DISCUSSION

From the perspective of tensile testing, the notch effects of the undercuts had a significant impact. Three specimens with more pronounced notches failed at those points. The sample, which was almost free of undercuts, fractured in the S355MC base material. Nevertheless, despite this fact, the forces required to cause failure were very similar.

Sample S3, which appeared to have the best undercut characteristics, was selected for the fatigue tests. Most of the specimens fractured at the weld toe in the undercut area. From this perspective, their notch effect—and likely also the notch effect of the sharp transition from BM to WM—was crucial. Undercut severity appeared to have a more pronounced effect on crack initiation than the increase in weld reinforcement observed at higher heat inputs. It would be useful to compare different welds of varying quality according to ISO 5817 and observe the impact on fatigue properties In this paper, welded joints were evaluated in Category C. However, the results for Categories B or D would be significantly different due to variations in geometry and, consequently, different input conditions, especially the notch effect (the greatest influence on fatigue properties).

In terms of hardness, notably, no significant softening was observed within the HAZ hardness relative to the BM; rather, the hardness from the WM decreases through the HAZ down to the level of the BM. As part of the analysis, the experimental results of the hardness map for the welded joint under evaluation were also compared with the results of the numerical analysis. A comparison of the profile and map results indicates that they are nearly identical. Figure 27 also includes a comparison of materials in terms of their mechanical properties, which in turn affects their hardness. Based on this, the results (numerical and also experimental) confirmed that the weld metal achieves the highest hardness values.

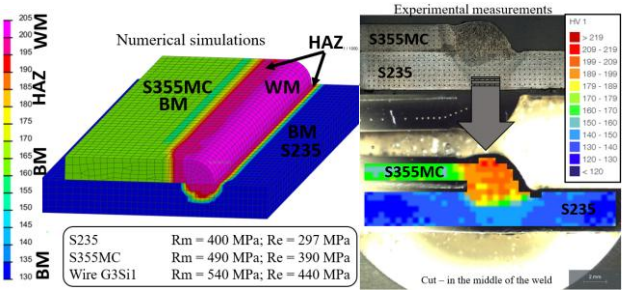


Figure 27. Hardness map – numerical and experimental measurements

Since the results of the hardness and tensile tests showed similar outcomes between the individual welded specimens, only one reference specimen was selected for the numerical simulations. This is sufficient for the assessment of the relevance of the results and their potential future applicability in terms of predicting results prior to the experiment itself.

The numerical simulations provided results that corresponded well with the experimental observations and reflected the expected behaviour of the welded joint.

The results indicate that the influence of heat input cannot be evaluated solely through hardness measurements or static tensile properties. Within the investigated range, only minor differences were observed in hardness distribution and maximum tensile force. In contrast, a substantially greater effect was observed in relation to weld geometry. The reduction of undercut severity with increasing heat input altered the preferred crack initiation sites and consequently affected fatigue behaviour. These observations confirm that local geometric stress concentrators play a dominant role in the fatigue response of welded lap joints.

One limitation of the numerical model is that it does not explicitly account for welding imperfections such as undercuts, pores or lack of fusion. Consequently, although the simulations provide valuable information regarding thermal history, phase evolution, hardness distribution and residual stress development, the experimentally observed fatigue behaviour remains strongly dependent on geometric discontinuities that cannot be fully represented by the present model.

6 CONCLUSIONS

This paper presents information on the welding of dissimilar lap joints in structural steels, supported by numerical simulations. The materials used in the experiments were S235JR (4 mm), S355MC (3 mm) and filler wire G3Si1 (1 mm). The MAG welding technology was used. The experimental results showed that:

- Increasing heat input reduced the severity of undercuts and simultaneously increased weld reinforcement and penetration depth.
- The presence of undercuts affected the location of the crack during tensile testing but did not significantly affect the force required to break the specimen.
- The presence of undercuts had a significant effect on the fracture location of the specimens during fatigue testing, with most of the welded joints fracturing exactly in these areas.
- The influence of heat input was manifested primarily through changes in weld geometry, whereas its effect on hardness distribution and static tensile behaviour remained limited.

- Despite cracking in the undercut areas of the specimens, the welds passed the fatigue testing (according to Category 614 of the IIW) for almost specified strain amplitudes (except for the maximum strain amplitude 85 MPa).
- The highest hardness was found in the weld metal, gradually decreasing within the BM to a certain level (there was no decrease in hardness in the HAZ below the BM values).
- The experimental results confirmed good agreement with the numerical simulations, demonstrating their applicability for predicting phase distribution, hardness evolution, deformation and residual stress development.

ACKNOWLEDGMENTS

Acknowledgements This work was supported by the Project for the Development of the Organization "VAROPS (DZRO VAROPS) Military autonomous and robotic assets" of the Ministry of Defence of the Czech Republic. Additional support was provided by the specific research SV26-216 at the Department of Mechanical Engineering, Faculty of Military Technology, University of Defence, and by specific research conducted at the Faculty of Mechanical Engineering, Brno University of Technology.

REFERENCES

[Hobbacher 2016] Hobbacher, A. F. Recommendations for fatigue design of welded joints and components: IIW document IIW-2259-15 ex XIII-2460-13/XV-1440-13: this document is a revision of XIII-2151r4-07/XV-1254r4-07. [online]. Second edition. IIW collection. Cham: Springer, [2016]. ISBN 978-3-319-23757-2. doi: https://ebookcentral.proquest.com/lib/techlib-ebooks/detail.action?docID=4206767. [cit. 2026-06-15].

[Kik 2024] Kik, T. Calibration of Heat Source Models in Numerical Simulations of Welding Processes. [online]. Metals 2024, 14, 1213. [15-06-2026] doi: https://doi.org/10.3390/met14111213.

[Kubicek 2016] Kubicek, J. et al. Welded joint of high-strength steels Weldox 700 and common grade steel S 355. MM Science Journal, 2016, vol. 2016, iss. 5, p. 1398-1401. ISSN: 1803-1269.

[Lang 2025] Lang, R. Fatigue life prediction of welded steel components based ongeometric scan data [online]. Steel Construction 2025, 18, No. 2, pp. 80–88. [15-06-2026] https://doi.org/10.1002/stco.202400050.

[Macdonald 2011] Macdonald, K. A. (ed.). Fracture and fatigue of welded joints and structures [online]. Cambridge: Woodhead Publishing, 2011. ISBN 978-1-84569-513-2. [cit. 2026-06-15].

[Muncut 2015] Muncut, E. et al. Structural Analysis for Joining Dissimilar Thin Sheets with CMT (Cold Metal Transfer) Process [online]. 2015, AMR 1111, 49–55. [15-06-2026] doi: https://doi.org/10.4028/www.scientific.net/amr.1111.49

[Mroz 2023] Mróz, M. et al. Numerical and Physical Simulation of MAG Welding of Large S235JRC+N Steel Industrial Furnace Wall Panel [online]. Materials 2023, 16, 2779. [15-06-2026] doi: https://doi.org/10.3390/ma16072779

[Nagasai 2024] Nagasai P. B. et al. Cold metal transfer technology - A review of recent research developments, Results in Engineering, [online]. 2024, Volume 23, 102423, ISSN 2590-1230, doi: https://doi.org/10.1016/j.rineng.2024.102423. (https://www.sciencedirect.com/science/article/pii/S2590123024006789)

[Mueller 2022] Mueller E., Hermann T. Formation of residual stresses at welding seams with s235 and s355. ICRS 11 - The 11th International Conference of Residual Stresses, SF2M; IJL, Mar 2022, Nancy, France. hal-04022500

[Oliveira 2021] Oliveira, A.S. et al. A Detailed Forecast of the Technologies Based on Lifecycle Analysis of GMAW and CMT Welding Processes. Sustainability [online]. 2021, 13, 3766. doi: https://doi.org/10.3390/su13073766

[Peric 2020] Perić, M. el al. Numerical Simulation and Experimental Investigation of Temperature and Residual Stress Distributions in a Circular Patch Welded Structure. Energies 2020, 13, 5423.

[Schmidt 2025] Schmidt, T. ESB-European Steel Business, 2025, Moers, Germany [online]. 2025 [15-06-2026]. doi: https://www.esb-group.com/en/products-din-en/hot-rolled-microalloyed-steel/s355mc-micro-alloyed-hot-rolled-steel-for-cold-forming/

[Stanciu 2017] Stanciu E.M. et al. CMT Welding of Low Carbon Steel Thin Sheets, Romania [online]. 2017 [15-06-2026]. IOP Conf. Ser.: Mater. Sci. Ing. 209 012051. doi: 10.1088/1757-899X/209/1/012051

[Stanisz 2022] Stanisz D. et al. Microstructure and Mechanical Properties of Joints Depending on the Process Used. Materials (Basel). 2022 Jul 26;15(15):5171. doi: 10.3390/ma15155171. PMID: 35897605; PMCID: PMC9332689.

CONTACTS:

Ing. et Ing. Martin Dostal[1], Ing. Marek Slovacek Ph.D. IWE[1], Ing. Petr Svoboda[2]
Brno University of Technology, Faculty of Mechanical Engineering,
Institute of Manufacturing Technology, [1]Department of Welding and Surface Treatment, [2]Department of Metal Forming and Welding Technologies
Technicka 2896/2, Brno, 616 69, Czech Republic
e-mail: 217110@vutbr.cz
e-mail: slovacek@fme.vutbr.cz
e-mail: 209148@fme.vutbr.cz

Ing. Mgr. Hana Sebestova Ph.D.
Institute of Scientific Instruments of the Czech Academy of Sciences, Brno, Czech Republic
Kralovopolska 147, Brno, 612 00, Czech Republic
e-mail: sebestova@isibrno.cz

Ing. Jindrich Vilis Ph.D., Ing. Martin Klimes

Faculty of Military Technology, University of Defence, Department of Engineering
Kounicova 65, 662 10 Brno. Czech Republic
e-mail: jindrich.vilis@unob.cz
e-mail: martin.klimes@unob.cz

LICENSE CREATIVE COMMONS:

The article is published under the terms and conditions of the Creative Commons Attribution 4.0 International License (CC BY 4.0).